This is natural since contracting forces act on the lower half of the ends of the beam. However, when the load parameter is increased further the value of σ_+ becomes positive – a stretching region occurs due to slip along the line L (curve 2, Fig. 4, $\Omega = 0.13$ and $\eta = 0.5$). Similar behavior of the stresses is observed in the upper half of the beam (see Fig. 4). Note that the variational formulations of the boundary-value problems [2] and the algorithm considered can also be used to solve problems on the development of cracks in normal fracture.

The author thanks E. I. Shemyakin and A. F. Revuzhenko for their interest and useful comments.

LITERATURE CITED

1. A. F. Reveuzhenko, S. B. Stazhevskii, and E. I. Shemyakin, "Asymmetry of plastic flow in a converging symmetrical channel," FTPRPI, No. 3 (1977).
2. A. F. Revuzhenko and E. I. Shemyakin, "Some formulations of boundary-value problems of L-plasticity," Zh. Prikl. Mekh. Tekh. Fiz., No. 2 (1979).
3. F. L. Chernous'ko and N. V. Banichuk, Variational Problems in Mechanics and Control [in Russian], Nauka, Moscow (1973).

NUMERICAL SIMULATION ON A COMPUTER OF THE PROCESS OF EXPLOSIVE FORMING

V. K. Borisevich, V. P. Sabel'kin, and S. N. Solodyankin

UDC 51.380.115:983.044

The problem of simulating the dynamic behavior of an axisymmetrical blank for explosive forming under plane stressed state conditions with rigid fastening or hinged rest on a contour is considered in a number of papers [1-4] (a detailed bibliography is given in [5]), and in [6] a method is described for determining the dynamic behavior of thin nonaxisymmetrical shells of ideally plastic material deformationally hardened and sensitive to the rate of deformation for the boundary conditions described above. In this paper we describe a method for the numerical calculation of the dynamic behavior of nonaxisymmetrical blanks of complex configuration. Unlike publications where problems unrelated to practice are solved, here we simulate the process of forming–drawing, taking into account both the displacement of the flange part of the blank and the forces of friction which occur on the flange part of the blank during high-speed deformation. In addition, as a result of an optimizational search the optimum external load applied to the blank is determined, which enables the values and positions of the charges required to deform it to be found.

1. The system of differential equations describing the motion of a blank (more accurately a Lagrange network, connected with its middle surface) can be written exactly as in [5] and can be solved in explicit form using the method of finite differences [7]. It turns out that the finite-difference model is sensitive to the integration step in time. In addition, the stability of the difference scheme depends on the initial value of the cell of the integration network. According to [8], the upper boundary of the integration step in time is expressed in the form

$$\Delta t = 2/\omega_{\max},$$

where $\omega_{\max}$ is the highest eigenfrequency of the corresponding finite-difference model. However, solving problems it is extremely inconvenient to determine in advance the frequency $\omega_{\max}$ corresponding to each specific finite-difference model. Hence, to determine Δt one can use the condition [5]

$$\Delta t \leqslant \Delta X_{\min}(\rho(1-\nu^2)/E)^{1/2},$$

where $\Delta X_{\min}$ is the value of the cell of the network, ρ is the density of the material of the blank, ν is Poisson's ratio, and E is Young's modulus. When integrating the equations at each subsequent instant of time one determines the displacement of the junction points of the Lagrange network. If at the initial instant of time $t = 0$ we write the equation of motion

$$F^j_{mn} = \bar{\rho}\ddot{Y}^j_{mn},$$

Kharkov. Translated from Zhurnal Prikladnoi Mekhaniki i Tekhnicheskoi Fiziki, No. 2, pp. 165-175, March-April, 1979. Original article submitted March 20, 1978.

where F^j_{mn} are the projections of the forces reduced to the junction point mn, $\ddot{Y}^j_{mn}$ are the projections of the accelerations of the junction points of the network, $\bar{\rho}$ is the reduced mass of a junction point, determined from the equation

$$\bar{\rho} = \rho\delta,$$

where δ is the thickness of the blank, the increment in the displacement at any subsequent instant of time is found from the Taylor expansion

$$(\Delta Y^j_{mn})_{i+1} \simeq (\Delta Y^j_{mn})_i + (\ddot{Y}^j_{mn})_i (\Delta t)^2, \text{where} (\Delta Y^j_{mn})_i = (\Delta \dot{Y}^j_{mn})_i (\Delta t).$$

The geometry of the blank is defined in terms of the basis vectors

$$\mathbf{A}^{mn,i}_\alpha = (Y^j_\alpha)^{mn,i}\, \mathbf{i}_j,$$

where $\mathbf{i}_j$ are the orthogonal basis vectors of a Cartesian coordinate system Y^j, while

$$(Y^j_\alpha)^{mn,i} = (\partial Y/\partial X^\alpha)_{mn,i}. \tag{1.1}$$

Here close to the boundaries the "forward" or "backward" differences are used, while inside the blank the "central" differences are used, where in the case considered for a rectangle in the plan of the blank the boundaries coincide with $X^1 = 1, \ldots, M$, $X^2 = 1, \ldots, N$, where m and n are the numbers of the junction points of the Lagrange network, and M and N are its maximum dimensions.

We will further determine the metric tensors, their determinants, the curvature tensors, the directions of the normals, and also the increments in the components of the deformation tensor

$$(\Delta\varepsilon_{\alpha\beta})^{mn}_{i+1} = 0.5\left[(A_{\alpha\beta})^{mn,i}_{i+1} - (A_{\alpha\beta})^{mn}_i\right] - X^3\left[(B_{\alpha\beta})^{mn}_{i+1} - (B_{\alpha\beta})^{mn}_i\right],$$

where $(A_{\alpha\beta})^{mn}$ and $(B_{\alpha\beta})^{mn}$ are the metric tensors and the curvature tensors, and α and β take the values 1 and 2.

Knowing the increment in the deformation at each step and the time during which it is obtained, we find the rate of deformation

$$(\dot{\varepsilon}_{\alpha\beta})^{mn}_{i+1} = (\Delta\varepsilon_{\alpha\beta})^{mn}_{i+1}/\Delta t$$

and the intensities of the rates of deformation

$$\dot{\varepsilon}^{mn}_{i+1} = \frac{2}{3}^{1/2}\left\{\left[(\dot{\varepsilon}_{11})^{mn}_{i+1}\right]^2 + \left[(\dot{\varepsilon}_{22})^{mn}_{i+1}\right]^2 + \left[(\dot{\varepsilon}_{12})^{mn}_{i+1}\right]^2 + \left[(\dot{\varepsilon}_{11})^{mn}_{i+1}(\dot{\varepsilon}_{22})^{mn}_{i+1}\right]\right\}^{1/2}$$

for taking into account both the deformational hardening and the sensitivity of the material of the blank to the rate of deformation [9] in terms of $\sigma_{sd} = \sigma_{s0}[1 + (\dot{\varepsilon}^{mn}/D)^{1/\chi}]$ where σ_{s0} is the yield point of the material for static loading, and D and χ are constants of the material determined experimentally.

In view of the fact that simulation of the explosive forming process is carried out mainly for thin blanks, Kirchnoff's hypotheses are completely applicable; namely: 1) the normal $\mathbf{N}_{mn}$ remains normal also to the deformed middle surface of the blank, 2) in the direction of this normal there is no deformation, although in the final analysis thinning of the blank is determined from the law of conservation of volume for each elementary cell, and 3) deformation of the transverse shift is zero. Although a change in the deformation along the thickness of a shell is also taken in accordance with Kirchnoff's assumption, their calculation is carried out for each layer separately. In this case the choice of four layers [5] over the thickness of the blank (where the material is concentrated), which works for the plane stressed state, is the optimum. These layers are situated at the same distance from one another and are separated by material which cannot operate under conditions of a plane stressed state in a plane tangential to the shell, but which possesses an infinitely large rigidity to shear in a transverse direction.

When determining the increments of deformation it is convenient to divide the latter into elastic and plastic components [10]:

$$\Delta\varepsilon_{\alpha\beta} = \Delta\varepsilon^e_{\alpha\beta} + \Delta\varepsilon^p_{\alpha\beta}.$$

In Cartesian coordinates Y^j the increment in stress in terms of the elastic component of the increment in deformation is given by the following equations:

$$\Delta\sigma_{11} = E\left(\Delta\varepsilon^e_{11} + \nu\Delta\varepsilon^e_{22}\right)/(1-\nu^2),$$

$$\Delta\sigma_{22} = E\left(\Delta\varepsilon^e_{22} + \nu\Delta\varepsilon^e_{11}\right)/(1-\nu^2),\quad \Delta\sigma_{12} = E\Delta\varepsilon_{12}/(1+\nu).$$

The yield condition is best used in the Mises–Hencky form

$$\Phi^{y}_{mn,i} = -3J_2^{mn,i} - (\sigma_{sd})^2_{mn,i} = 0, \tag{1.2}$$

where $\Phi^{y}_{mn,i}$ is the yield function, and $J_2^{mn,i}$ is the second invariant of the stress deviator. In our case Eq. (1.2) takes the form

$$\Phi^{y}_{mn,i} = -\sigma^{mn}_{11,i}\sigma^{mn}_{22,i} + 3\sigma^{mn}_{12,i}\sigma^{mn}_{21,i} + (\sigma^{mn}_{11,i})^2 + (\sigma^{mn}_{22,i})^2 - (\sigma^{mn}_{sd,i})^2. \tag{1.3}$$

For an absolutely elastic–plastic material the plastic components of the deformation increment tensor are related to the stresses in terms of the flow law, which, according to the theory of plastic potential [11], can be expressed in the form

$$\Delta e^{p}_{\alpha\beta,mn,i} = \vartheta^{mn}_{i}\partial\Phi^{y}_{mn,i}/\partial\sigma^{mn,i}_{\alpha\beta},$$

where ϑ^{mn}_{i} is a positive constant found from Eq. (1.3) by substituting into the latter the values of the stresses obtained taking into account the elastic and plastic components of the deformation tensor. At each i step, if there is plastic flow inside the region of values of limiting deformations, the end of the stress vector returns to the yield surface $\Phi^{y}_{mn,i}$.

After determining the stresses (for each layer) we calculate the values of the membrane forces $H^{\alpha\beta}_{mn,i}$ and the bending moments $L^{\alpha\beta}_{mn,i}$ for each junction point in the initial nondeformed Cartesian system of coordinates in the same way as for the components of the deformation increments:

$$H^{\alpha\beta}_{mn,i} = \int_{-0,5\delta}^{0,5\delta} \sigma^{\alpha\beta}_{mn,i}\, dX^3_{mn,i}, \quad L^{\alpha\beta}_{mn,i} = \int_{-0,5\delta}^{0,5\delta} \sigma^{\alpha\beta}_{mn,i} X^3_{mn,i}\, dX^3_{mn,i}.$$

The integration is best of all carried out using Gauss's quadrature formulas using standard subroutines of the type described in [12].

The equation of equilibrium for the moments can be written in the form

$$\partial_\beta L^{\alpha\beta}_{mn,i} + \left\{\begin{matrix}\alpha\\ \gamma\beta\end{matrix}\right\}_{mn,i} L^{\gamma\beta}_{mn,i} + \left\{\begin{matrix}\beta\\ \gamma\beta\end{matrix}\right\}_{mn,i} L^{\alpha\gamma}_{mn,i} = Q^{\alpha}_{mn,i}, \tag{1.4}$$

where $Q^{\alpha}_{mn,i}$ is the cutoff force expressed in the brackets – the Christoffel symbols of the second kind

For $\alpha = 1$ Eq. (1.4) takes the form

$$\begin{aligned} Q^1_{mn,i} = {} & \partial L^{11}_{mn,i}/\partial X^1_{mn,i} + \mathbf{A}^1_{mn,i}\cdot(\partial \mathbf{A}^{mn,i}_1/\partial X^1)\, L^{11}_{mn,i} + \\ & + \mathbf{A}^1_{mn,i}\cdot(\partial \mathbf{A}^{mn,i}_2/\partial X^1)\, L^{21}_{mn,i} + \mathbf{A}^1_{mn,i}\cdot(\partial \mathbf{A}^{mn,i}_1/\partial X^1)\, L^{11}_{mn,i} + \\ & + \mathbf{A}^1_{mn,i}\cdot(\partial \mathbf{A}^{mn,i}_2/\partial X^1)\, L^{12}_{mn,i} + \partial L^{12}_{mn,i}/\partial X^2 + \mathbf{A}^1_{mn,i}\cdot(\partial \mathbf{A}^1_{mn,i}/\partial X^2) \times \\ & \times L^{12}_{mn,i} + \mathbf{A}^1_{mn,i}\cdot(\partial \mathbf{A}^{mn,i}_2/\partial X^2)\, L^{22}_{mn,i} + \mathbf{A}^2_{mn,i}\cdot(\partial \mathbf{A}^{mn,i}_1/\partial X^2) \times \\ & \times L^{11}_{mn,i} + \mathbf{A}^2_{mn,i}\cdot(\partial \mathbf{A}^{mn,i}_2/\partial X^2)\, L^{12}_{mn,i}. \end{aligned} \tag{1.5}$$

Similarly for $\alpha = 2$. If the network is nonuniform, in Eq. (1.5) instead of ∂X^1 and ∂X^2 we must write ∂X^1_m and ∂X^2_n. The finite difference representation of Eq. (1.4) is constructed in the same way as for (1.1).

Knowing the membrane forces, the bending moments, and the cutoff forces the acceleration of the junction points of the network can be found from the equations of motion [5]

$$\begin{gathered} \nabla_\beta H^{\beta\alpha}_{mn,i} - Q^{\beta}_{mn,i} B^{\alpha}_{\beta,\, mn,i} + F^{\alpha}_{mn,i} + G^{\alpha}_{mn,i} = \bar{\rho}\ddot{\mathbf{Y}}^{\alpha}_{mn,i}, \\ H^{\beta\alpha}_{mn,i} B^{mn,i}_{\alpha\beta} + \nabla_\beta Q^{\beta}_{mn,i} + F^{3}_{mn,i} = \bar{\rho}\ddot{\mathbf{Y}}^{3}_{mn,i}, \end{gathered}$$

which, after some simple reduction, give

$$\ddot{Y}^{j}_{mn,i} = \left[A^{\frac{1}{2}}_{mn,i}/\left(\bar{\rho}_0 A^{\frac{1}{2}}_{mn,0}\right)\right]\left[F^{j}_{mn,i} + \partial C^{\beta j}_{mn,i}/\partial X^{\beta} + A^{\beta}_{mn,i} C^{\gamma j}_{mn,i}(\partial A^{mn,i}_{\gamma}/\partial X^{\beta})\right],$$

where $A_{mn,0}$ and $A_{mn,i}$ are the determinants of the metric tensors, and $C^{\beta j}_{mn,i}$ is the surface-space tensor defined from the equation

$$C^{\beta j}_{mn,i} = H^{\beta\alpha}_{mn,i} Y^{j}_{\alpha,mn,i} + Q^{\beta}_{mn,i} N^{j}_{mn,i},$$

where $N^{j}_{mn,i}$ are the projections of the normal onto the junction point mn.

TABLE 1

$\widetilde{F}_{mn1}$		m											
		1	2	3	4	5	6	7	8	9	10	11	12
n	1	0	0	0	0	0	0	0	0	0	0	0	0
	2	0	0	0	0	0	0	0	0	0	0	0	0
	3	0	0	0	0	0	0	0	0	0	0	0	0
	4	0	0	0	0,692	0,733	0,772	0,814	0,843	0,870	0,900	0,907	0,907
	5	0	0	0	0,703	0,750	0,794	0,831	0,870	0,907	0,920	0,937	0,955
	6	0	0	0	0,730	0,772	0,813	0,856	0,900	0,919	0,955	0,965	0,978
	7	0	0	0	0,733	0,782	0,822	0,870	0,906	0,937	0,965	0,978	1
	8	0	0	0	0,733	0,782	0,822	0,870	0,906	0,906	0,955	0,978	1

TABLE 2

i	1	2	3	4	5	6	7	8	9	10	11	12	13
$\widetilde{F}^{*}_{128i}$	1	0,757	0,577	0,461	0,365	0,295	0,250	0,218	0,205	0,198	0,186	0,173	0,166
i	14	15	16	17	18	19	20	21	22	23	24	25	26
$\widetilde{F}_{128i}$	0,166	0,147	0,141	0,128	0,115	0,103	0,083	0,070	0,038	0,019	0,010	0,005	0,001

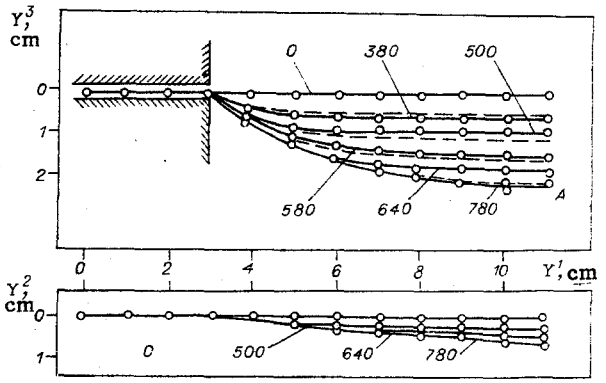

Fig. 1

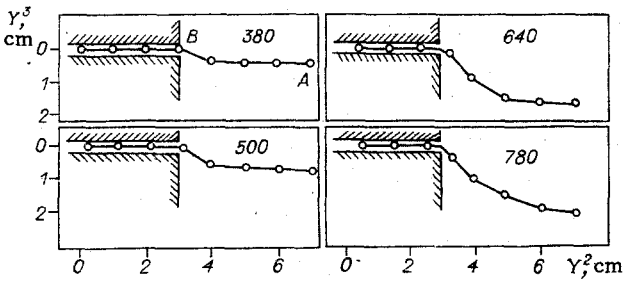

Fig. 2

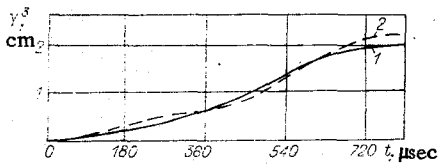

Fig. 3

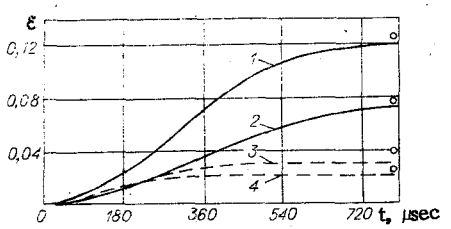

Fig. 4

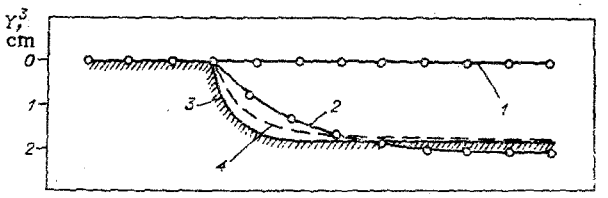

Fig. 5

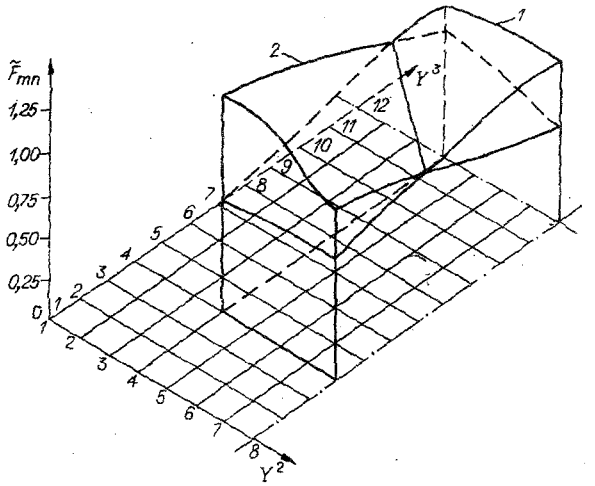

Fig. 6

After calculating the accelerations $\ddot{Y}^j_{mn,i}$ the increments of the displacements and the new positions of the Lagrange networks are found, and the calculation procedure is repeated cyclically.

2. As was pointed out in [3, 4], when simulating the dynamic behavior of the blank during forming–drawing, neglect of the forces of friction on the flange part of the blank introduces considerable error into the calculation. In this paper this drawback is eliminated using the hydrodynamic theory of friction. Here the force of friction is defined by Petrov's formula [13]

$$G = \eta \dot{Y}_S S/(h + \eta/\mu_1 + \eta/\mu_2),$$

where η is the viscosity of the lubricating layer, $\dot{Y}_S$ is the rate of slip, S is the area of the flange part of the blank, h is the thickness of the lubrication layer, and μ_1 and μ_2 are the coefficients of the external friction of the lubrication and of the slipping surface.

When the lubrication and the slipping surfaces of the blank and the matrix have high adsorption properties, the quantities η/μ_1 and η/μ_2 can be neglected [13]. Equation (2.1) then takes the form

$$G = \eta \dot{Y}_S S/h.$$

If the flange part of the blank has pq junction points we have

$$(G_{pq})^{i+1} = 2\eta S_{pq} (\dot{Y}^j_{pq})^i/h,$$

where $(G_{pq})^{i+1}$ is the force of friction applied from both sides to the junction pq, S_{pq} is the area of the cell, and $(\dot{Y}^j_{pq})$ is the rate of displacement of the junction point.

3. The main question considered in problems of explosive forming is the problem of the external load applied impulsively to the blank. In [14] the semiinverse problem of the deformation, consisting of determining the form of the initial applied pulse with respect to a specified finite configuration of an axisymmetrical shell, is considered. Unlike the problem considered in the semiinverse formulation, in the present paper the external load necessary to form nonaxisymmetrical components of complex configuration is determined by the method of optimizational search. In this case the initial shape of the blank is plane, a cylinder, or a cone of constant thickness, if the first transition of deformation is simulated, or any complex spatial shape with a certain thickness distribution when simulating subsequent transitions.

Suppose the initial impulse applied to the blank is written in the form

$$\mathbf{I}_0 = \sum_{m=1}^{m=M} \sum_{n=1}^{n=N} \sum_{i=1}^{i=k} \mathbf{F}_{mni} \cdot \Delta t_{i},$$

where $\mathbf{F}_{mni}$ is the force reduced to the junction point of the network of the middle surface of the blank.

Applying the initial impulse $\mathbf{I}_0$ to the deformed blank using the method described in Secs. 1 and 2, we will simulate its dynamic behavior and determine the final buckling of the blank. Now, knowing the final buckling of the blank and the profile of the matrix, we set up the quadratic Gauss functional

$$\Gamma(\mathbf{I}_0) = \sum_{m=1}^{m=M} \sum_{n=1}^{n=N} (N_{mn})^2, \tag{3.1}$$

where N_{mn} is the length of the normal from the mn junction point to the surface of the matrix, determined from the relation

$$N_{mn}(I_0) = [(N^1_{mn})^2 + (N^2_{mn})^2 + (N^3_{mn})^2.$$

The problem of determining the external load now reduces to minimizing the functional (3.1) on the family of curves I(F, t). We will use Newton's method for this purpose [15] with a modification when determining the displacement in the direction of the optimum point at each step. To simplify the solution we will assume that

$$\Delta t_i = \Delta t = \text{const},$$

when the direction of search is defined only with respect to $\mathbf{F}_{mni}$. If we denote by $\Delta \mathbf{F}^{\xi}_{mni}$ the increment of the force $\mathbf{F}^{\xi}_{mni}$ at the mn junction point of the Lagrange network at the i-th instant of time at the ξ-th iteration step, we have

$$\Delta F^{\xi}_{mni} = F^{\xi+1}_{mni} - F^{\xi}_{mni}. \tag{3.2}$$

Here and henceforth the index ξ will denote the iteration step. We expand the functional in a Taylor series and neglecting terms of the third and higher orders, we write

$$\Gamma(\mathbf{F}^{\xi+1}_{mni}) = \Gamma(\mathbf{F}^{\xi}_{mni}) + \nabla^{y}\Gamma(\mathbf{F}^{\xi}_{mni})\,\Delta F^{\xi}_{mni} + 0{,}5\,(\Delta F^{\xi}_{mni})^{y}\nabla^2\Gamma(\mathbf{F}^{\xi}_{mni})\cdot\Delta F^{\xi}_{mni},$$

where $\nabla^{y}\Gamma(\mathbf{F}^{\xi}_{mni})$ is the transposed matrix of the gradients of the first order

$$\nabla\Gamma(\mathbf{F}^{\xi}_{mni}) = \left\| \frac{\partial\Gamma(\mathbf{F}^{\xi}_{mni})}{\partial F^{\xi}_{kli}} \right\|;$$

$\nabla^2\Gamma(\mathbf{F}^{\xi}_{mni})$ is the cubic matrix of the second partial derivatives

$$\nabla^2\Gamma(\mathbf{F}^{\xi}_{mni}) = \| \nabla^2_{kl}\Gamma(\mathbf{F}^{\xi}_{mni}) \|,$$

where $\nabla^2_{mn}\Gamma(\mathbf{F}^{\xi}_{mni})$ is defined by the matrix

$$\nabla^2_{mn}\Gamma(\mathbf{F}^{\xi}_{mni}) = \left\| \frac{\partial^2\Gamma(\mathbf{F}^{\xi}_{mni})}{\partial F^{\xi}_{kli}\,\partial \mathbf{F}^{\xi}_{mni}} \right\|.$$

The minimum of the functional in the direction $\Delta\mathbf{F}^{\xi}_{mni}$ is determined by differentiating $\Gamma(\mathbf{F}^{\xi}_{mni})$ with respect to each of the components $\Delta\mathbf{F}^{\xi}_{mni}$ and equating the expressions obtained to zero. This leads to

$$\Delta F^{\xi}_{mni} = -[\nabla^2\Gamma(\mathbf{F}^{\xi}_{mni})]^{-1}\cdot\nabla\Gamma(\mathbf{F}^{\xi}_{mni}). \tag{3.3}$$

We will express the quantity $\mathbf{F}^{\xi+1}_{mni}$ from Eq. (3.2) and substitute the value of $\Delta\mathbf{F}^{\xi}_{mni}$ from (3.3). We finally obtain

$$F^{\xi+1}_{mni} = F^{\xi}_{mni} - [\nabla^2\Gamma(\mathbf{F}^{\xi}_{mni})]^{-1}\cdot\nabla\Gamma(\mathbf{F}^{\xi}_{mni}). \tag{3.4}$$

In Eq. (3.4) the operation of matrix inversion is present, which can conveniently be carried out using standard MINV subroutines [12], since we must ensure that it is positive-definite. In this case, when it is not positive-definite (such situations may arise in special cases), some authors assume additional transformations making the inverse matrix positive-definite at each step of the minimization [16].

We will not consider the optimizational search in the direction Δt_i in this version since in this case to ensure similarity of the impulsive action it is necessary to impose special limitations on the value of the step

with respect to Δt_i, otherwise it acquires a character which it is impossible to ensure for any conditions of explosive deformation.

4. To check the theoretical assumptions regarding this method we compiled a FORTRAN program and carried out a numerical simulation of the first transition of explosive forming of a component of the box type on the ES-1020 and ES-1033 computers. The blank was chosen to be a plane plate of rectangular shape in plan with dimensions $220 \times 140 \times 2.0$ mm^3 of AMg2-M aluminum alloy. A uniform grid with a step of 10 mm covered the whole plane of the blank. Although the problem considered in this case was symmetrical with respect to the longitudinal and transverse axes of the blank, the solution was carried out for all components, which enabled us to check the correctness of the solution with respect to the corresponding parameters at symmetrical points. The main initial data was as follows: yield stress $\sigma_{s0} = 7.85 \cdot 10^7$ Pa, Young's modulus $E = 6.97 \cdot 10^{10}$ Pa, Poisson's ratio $\nu = 0.33$, deformational strength indices $\lambda = 0.996$, $w = 0.15$, kinematic strength indices $D = 5.62 \cdot 10^6$ sec^{-1}, $\chi = 3.75$, limit dynamic deformation $\psi = 33\%$, and coefficient of dynamic viscosity of the lubricating layer $\eta = 800$ P. Because of the fact that the forces of friction [13] arising on the constricted rib of the matrix exceed the value of the forces of friction on the plane of the flange by a factor of 3 on the average, in the simulation they were increased by a specified amount compared with the theoretical value and were applied to the junction points closest to the constricted rib. The external load applied to the deformed blank was found by experiment when blasting a spherical charge of explosive close to the rigid boundary surfaces.

Table 1 shows values of the external load at the first instant of time for the fourth deformed blank. For convenience the forces F_{mn1} acting at an arbitrary junction point of the blank are expressed in fractions of the load applied at the central point of the blank F_{1281}:

$$\tilde{F}_{mn1} = F_{mn1}/F_{12\,8\,1},\ F_{12\,8\,1} = 39\text{MPa}.$$

The change in the forces with time for the central point is shown in Table 2, where

$$\tilde{F}_{12\,8i} = F_{12\,8i}/F_{12\,8\,1}.$$

At the remaining points of the blank the change of the load is the same.

Figure 1 illustrates the position both of points of the formed blank lying in the longitudinal plane of symmetry (the upper part), at discrete instants of time, and at points lying on the boundary of the flange part; the continuous lines represent the results of experimental investigations, and the dashed lines the results of numerical simulation. We indicate corresponding instants of time from the beginning of displacement (for the experiment: 0, 380, 500, 580, 640, 780 μsec) and from the beginning of the calculation (for the numerical simulation: 0, 380, 500, 580, and 780 μsec). Similar graphs for points lying in the transverse plane of symmetry are shown in Fig. 2. For different instants of time they are spaced, since, as numerical simulation and subsequent experiments showed, there is a considerable displacement of the external edge of the blank from the larger of its sides, whereas no displacement was observed from the smaller of its sides. The displacements of the central point of the blank (point A in Figs. 1 and 2) as a function of time are shown in Fig. 3, lines 1 showing the theoretical displacements obtained by numerical simulation, and lines 2 the results of experiment; it can be seen that the experimental curve, unlike the theoretical curve, despite the satisfactory overall agreement, has a number of features in the form of weak bends. The calculated nature of the motion is similar to that given in [17], but does not have singularities. Because of the fact that the external load in the experimental part of the work was generated in the region of rigid boundary surfaces, here there is a double loading of the moving blank: the first time by the hydroflow when the gaseous cavity expands, and the second due to the action of the jet when the cavity collapses [18]. Best results with respect to values of the final bucklings are achieved when the spatial grid is finely divided close to the constricted rib (X^1_{m4}, X^2_{m12}, X^2_{4n}, X^2_{20n}).

Figure 4 shows the dependence of the longitudinal and transverse deformations on the time in the region of points A and B (see Figs. 1 and 2). Here curve 1 is for ε^A_{11}, curve 2 is for ε^A_{22}, curve 3 is for ε^B_{11}, and curve 4 is for ε^B_{22}, and the points denote the final states of the experiment. As can be seen from the graphs, the increase in the deformations occurs smoothly, similar to the increase in the displacements of the central point of the blank. In this case the increase in the deformations at the point B occurs more intensively than at point A, which indicates the direction of motion of the plastic wave from the flange to the center of the blank. A numerical calculation was made up to the instant when the blank stops (450 steps in time); the simulation time was 56 minutes on the ES-1033 computer. It is possible to reduce the calculation time by using the symmetry of the blank, and, in addition, on computers with an increased memory it is possible to reduce the time taken in the repetitive carrying out of certain programs connected with determining the derivatives with respect to the spatial coordinates. It should be noted that unlike the statement made in [5] regarding the possibility of carrying out the calculation with the usual accuracy during numerical simulation when determining the basis vectors and other elements of differential geometry, and also the partial derivatives in finite-difference form, the need

arises to use double accuracy (up to the sixteenth decimal place), since calculations with the usual accuracy lead to considerable error accumulation and inadmissible errors in calculation already by the hundredth step. The increase in the error progressed when simulating the first transitions of the stamping, particularly when the blank was a flat plate.

The results of the optimizational search carried out using the algorithm proposed in Sec. 3 are shown in Figs. 5 and 6. In this case the initial pulse applied to the blank at the first step of the iteration is taken from Tables 1 and 2. The required final contour of the article determined by the surface of the matrix, was specified in tabular form with subsequent polynomial approximations by parts. Figure 5 shows: 1) the cross section of the blank before forming, 2) the position of the blank after simulation of the first transition of the forming as a result of applying a load (see Tables 1 and 2), 3) the forming contour of the matrix, and 4) the profile of the article obtained due to the action of the optimum load. The profile of the latter is shown in Fig. 6, where 1 is the initially applied load and 2 is the optimum force after five iteration steps; it can be seen that the increase in the load is more intensive in the region of the constricted ribs, particularly in the region of junction points, and this is completely confirmed in practice in forming block-shaped articles.

However, as the calculations showed, an increase in the load close to the constricted ribs is only possible up to a certain value, which depends on the radius of the constricted rib, the material and thickness of the blank, and the forces of friction on the flange part. Thus, when the load is reduced in the region X^1_{m4}, X^1_{m12}, X^2_{4n}, X^2_{20n} a considerable increase in the functional $\Gamma(F^{\zeta}_{mni})$ was observed due to the increase in the sum (3.1) in the region of the junction points. An increase in the load in the region up to values of 1.35 led to a breakdown of the continuity of the blank. Hence, Fig. 6 shows the limiting possible load for which, under the condition simulated, the plastic possibilities of the material of the blank are exhausted. We can therefore conclude that it is impossible to form an article of the profile shown in Fig. 5 in a single transition. For complete forming of the profile it is necessary to subject it to an impulsive action again.

LITERATURE CITED

1. B. A. Shcheglov, "Dynamics of axisymmetrical forming of thin-walled shells," in: Calculations of Plastic Flow Processes in Metals [in Russian], Nauka, Moscow (1973).
2. V. I. Bazaikin and V. N. Peretyat'ko, "Stress-deformed state of a circular membrane in dynamics," Zh. Prikl. Mekh. Tekh. Fiz., No. 4 (1975).
3. R. Osias, "User's guide for analysis of finite elastoplastic deformation," NASA, Cleveland, Ohio, 44135, Rep. E-7610 (June, 1974).
4. E. Boyd, "Dynamic deformations of circular membranes," J. Eng. Mech. Div., NEM3, (June, 1966), 1-16.
5. Moreno, W. Leech, and A. Witmer, "A more accurate method for the numerical calculation of nonstationary processes in elastoplastic thin shells for large deformations," Prikl. Mekh., No. 2, 131-144 (1971).
6. W. Leech, A. Witmer, and H. Pina, "Numerical calculation technique for large elastic–plastic transient deformations of thin shells," AIAA, No. 12, 2352-2359 (1968).
7. S. K. Godunov and V. S. Ryaben'kii, Introduction to the Theory of Difference Schemes [in Russian], Fizmatgiz, Moscow (1962).
8. W. Leech, Su, and Mack, "Stability of the method of finite differences for solving matrix equations," Raketn. Tekh. Kosm., No. 11, 27 (1965).
9. N. Jones, "Finite deflection of a rigid-viscoplastic strain hardening annular plate loaded impulsively," J. Appl. Mech. 35, No. 4, 344-356 (1968).
10. A. Witmer, A. Balmer, W. Leech, and H. Pian, "Large dynamic deformation of beams, rings, plates, and shells," AIAA J, 1, No. 8, 1848-1856 (1963).
11. L. Mal'vern, "Propagation of longitudinal plastic waves taking the rate of deformation into account," Mekhanika, Issue 1, No. 11 (1952).
12. Software for the ES Computer [in Russian], No. 4, Inst. Mat. Akad. Nauk BSSR, Minsk (1974).
13. E. I. Isachenkov, Forming of Rubber and Liquid [in Russian], Mashinostroenie, Moscow (1967).
14. V. D. Koshur, "Dynamic distortion of thin axisymmetrical shells under impulsive loading," in: Dynamics of a Continuous Medium [in Russian], No. 29, Inst. Gidrodinam. Sib. Otd. Akad. Nauk SSSR, Novosibirsk (1977).
15. D. Himmelblau, Applied Nonlinear Programming [Russian translation], Mir, Moscow (1975).
16. J. Greenstadt, Math. Comput., No. 21, 360 (1967).
17. M. A. Anuchin, O. D. Antonenkov, et al., "The motion of a blank under free forming by explosion," Izv. Vyssh. Uchev. Zaved., Mashinostr., No. 6, 155-161 (1963).
18. M. A. Faruqi, "Metal forming with underwater explosion bubbles located between rigid and free surfaces," Int. J. Mach. Tool Des. Res., 16, No. 4, 319-324 (1976).